ACS Catalysis

Research Article

pubs.acs.org/acscatalysis

How Can Fluctional Chiral Lanthanide (III) Complexes Achieve a High Stereoselectivity in Aqueous Mukaiyama-Aldol Reaction?

Miho Hatanaka*,† and Keiji Morokuma*

Fukui Institute for Fundamental Chemistry, Kyoto University, Kyoto 606-8103, Japan

Supporting Information

ABSTRACT: The aqueous Mukaiyama-Aldol reaction catalyzed by lanthanide (Ln) Lewis acid is one of the most attractive reactions for green chemistry. One of the chiral catalysts that achieved a high stereoselectivity is Ln^{3+} complexed with fluctional DODP, (2*R*,2′*R*)-dialkyl 2,2′-(1,7-dioxa-4,10-diazacyclododecane-4,10-diyl)dipropanoates. In this study, we theoretically studied the structure of the Ln^{3+}−DODP (Ln = Eu) complex and the transition states (TSs) for stereodetermining C−C bond formation step between benzaldehyde and silyl enol ether catalyzed by this complex to elucidate the origin of stereoselectivity of the reaction. To explore the local minima and TSs exhaustively, we used an automated exploration method, called the Global Reaction Root Mapping (GRRM) strategy. Unlike conventional rigid chiral catalysts, three conformers of the Eu^{3+}−DODP (the lowest **A**, the second lowest **B**, and the third lowest **C**) coexisted in the reaction system. Considering all the TSs obtained from the three conformers, we reproduced the experimental enantio excess and diastereomeric ratio quantitatively. The most stable TS for the C−C bond formation producing the major stereoisomer (*R*,*R*) was obtained from the second lowest conformer **B**. The lowest TS producing the enantiomer (*S*,*S*) was obtained from the conformer **C**; the similar (*S*,*S*) TS obtained from the conformer **B** was 0.4 kcal/mol less stable. Thus, to improve the enantioselectivity, the existing probability of the conformer **C** had to be reduced. The easiest way to achieve this is replacing Eu^{3+} by other Ln^{3+} with larger ionic radii, which was consistent with the experimental facts.

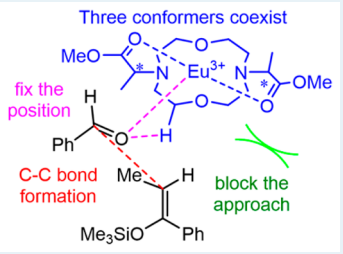

KEYWORDS: *asymmetric reaction, Lewis acid catalyst, aqueous media, Global Reaction Root Mapping, density functional theory*

INTRODUCTION

Catalytic reactions in aqueous media have recently been one of the most important topics for green chemistry.[1−6] Although conventional Lewis acid catalysts are inactive in water, a number of water-tolerant Lewis acid catalysts have been reported.[7−9] Lanthanide (Ln) complexes fit into this group of catalysts. Ln trication (Ln^{3+}) catalysts were in fact used in the first report of aqueous C−C bond formation, the so-called Kobayashi modification of Mukaiyama-Aldol reaction,[10,11] and have been used in many aqueous reactions.[7−14] Stereoselective reactions in aqueous media have also been reported with chiral ligands that are quite different from those widely used under anhydrous conditions.[15−19] One of the distinct chiral ligands is crown ether derivatives.[20−24] Allen and co-workers used the chiral complex of fluctional C_2 symmetric (2*R*,2′*R*)-dialkyl 2,2′-(1,7-dioxa-4,10-diazacyclododecane-4,10-diyl)dipropanoates, abbreviated here as DODPs, and achieved highly enantio- and diastereoselective aqueous Mukaiyama-Aldol reaction between benzaldehyde and silyl enol ether, as shown in Scheme 1.[22−24] Complexes of related DOTAs (1,4,7,10-tetraazacyclododecane-*N*,*N*′,*N*″,*N*‴-tetraacetic acid) derivatives with Ln^{3+}, although never applied as catalysts, have been widely used for in vivo luminescent probes[25−27] and MRI contrast agents,[28−35] and their structures and chemical properties have been studied both experimentally[28−35] and theoretically.[36,37] According to these studies, achiral Ln^{3+}-DOTA has four stereoisomers, two pairs of enantiomers (as shown in Figure S1 in Supporting Information (SI)), and the existing probability of each conformer depends on Ln^{3+}. Additionally, their chemical properties, such as the rate of water exchange on Ln^{3+}, depend on the stereoisomers. Therefore, the chiral Ln^{3+}−DOTA derivatives or Ln^{3+}−DODPs may also have several conformers whose properties are different from each other. Here are two major questions. If several conformers of a fluctional catalyst coexist in the reaction system, do all the conformers catalyze the reaction in the same way or different ways? How can such a fluctional catalyst

Scheme 1. Aqueous Mukaiyama-Aldol Reaction Catalyzed by Chiral Eu^{3+}-(*R*,*R*)−DODP

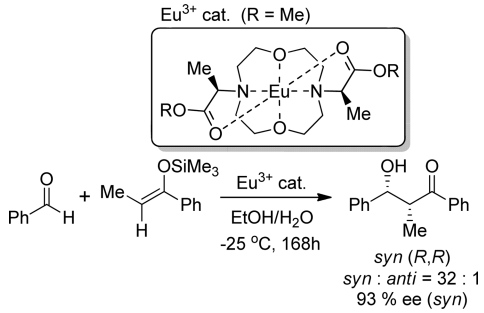

Received: March 1, 2015
Revised: May 1, 2015
Published: May 5, 2015

DOI: 10.1021/acscatal.5b00438
ACS Catal. 2015, 5, 3731−3739

achieve highly stereoselective reaction? This situation is totally different from conventional rigid catalytic systems that have only one stable structure.

To gain insights into the origin of stereoselectivity, a number of experimental conditions were examined, and the following three points were noted.[22−24] First, the product yield depends on substituents on two esters in the catalyst (R in Scheme 1). The luminescence decay measurement showed that two water and one aldehyde molecule coordinated to Eu^{3+} for normal alkyl-substituted catalysts, such as R = *n*-C_nH_{2n+1} (n = 1−4), and such catalysts achieved high yield and stereoselectivity. In contrast, catalysts with bulky substituents, such as R = *i*-Pr and *t*-Bu, or too small substituents, such as H, had three coordination water molecules and almost no aldehyde, which resulted in notably low yield. Second, a broad substrate scope was observed. High stereoselectivity was achieved both for aromatic and aliphatic aldehydes.[22,23] Third, the stereoselectivity depends on Ln^{3+} and was slightly improved by replacing Eu^{3+} with Nd^{3+}.[23] In spite of a number of studies, the origin of stereoselectivity has not been understood.

Computational chemistry has contributed substantially to elucidation of the origin of the stereoselectivity. However, despite their utility and interest, only few computational studies have been made for the water-tolerant Ln catalytic reactions.[38,39] One reason for the difficulty in computational study of such reactions is the structural fluctuation around Ln^{3+}. Ln^{3+} has a particular electronic configuration, such as $1s^22s^2\cdots 4f^N5s^25p^6$, in which open-shell 4f electrons are shielded by closed-shell 5s and 5p electrons from the outside. These inner-shell 4f electrons cannot form covalent bonds with surrounding ligands, and the Ln^{3+}-ligand bonds usually have a strong ionic bonding character. Therefore, there could be a number of transition states (TSs) as well as local minima (LMs) whose structures are slightly different from each other. In conventional computational studies, only a few TSs of stereodetermining step are computed and used to discuss the origin of stereoselectivity. This is enough for geometrically rigid systems. However, for fluctional systems, there could be a large number of TSs with slightly different structures and energies, many of which may contribute to the stereoselectivity.

The Global Reaction Route Mapping (GRRM) strategy[40] is ideally suited to address theoretically the problem of structural fluctuation. This strategy consists of two independent search methods, the anharmonic downward distortion following (ADDF) method[41−43] and the artificial force induced reaction (AFIR) method.[44,45] The ADDF method finds all LMs (isomers) and isomerization TSs starting from one or few LMs. The AFIR finds important approximate reaction pathways starting from LMs or dissociation limits, from which true reaction pathways (TSs and intermediates) are optimized. In our recent theoretical studies, we applied the GRRM strategy to Kobayashi-modification of Mukaiyama-Aldol reaction between benzaldehyde and trimethlysilyl (TMS) cylcohexenolate catalyzed by $Eu^{3+}(H_2O)_8$[10,11] and succeeded in clarifying the reaction mechanism and answering two unsolved questions about the role of water.[38,39] We have found that this reaction proceeds via a stepwise mechanism: the first step is C−C bond formation, followed by proton transfer from a first-shell water molecule to benzaldehyde, and then TMS dissociation caused by nucleophilic attack by bulk water molecules. The stereoselectivity of this reaction is determined at the C−C bond formation step. To identify the stereodetermining TSs exhaustively, we applied the AFIR method and found 96 and 71 TSs that produce *syn*- and *anti*-structures, respectively. That is to say that the GRRM strategy successfully sampled conformational space of C−C bond formation as well as coordination space of many first-shell water molecules, without running very expensive molecular dynamics calculations. Among 167 TSs, 17 lower TSs were found to contribute in reproducing the experimental diastereomeric ratio quantitatively.[38]

In the present study, we show how the fluctional DODP ligand−Eu^{3+} complex achieves a high enantio- and diastereoselectivity in the aqueous Mukaiyama-Aldol reaction. First, we explore all possible conformers of the chiral Eu^{3+}−DODP complex by the ADDF method. Then we will find stable prereaction intermediates with an aldehyde and coordination water molecules around Eu^{3+}. Based on the obtained stable intermediates, we search all important TSs of stereodetermining C−C bond formation step using the AFIR method and discuss the origin of the stereoselectivity. At the end, we propose a possible way of improving the enantioselectivity.

RESULTS AND DISCUSSION

Different Conformations and Distribution of Eu^{3+}−DODP Catalyst. As will be described in the Computational Details section, the ADDF method[41−43] was used to find all possible conformers of the Eu^{3+} chiral catalyst, and 24 conformers were actually obtained. Figure 1 shows the five lowest conformers **A**−**E**. (See Table S1 and Figure S2 in Supporting Information (SI) for other conformers **F**−**T**.)

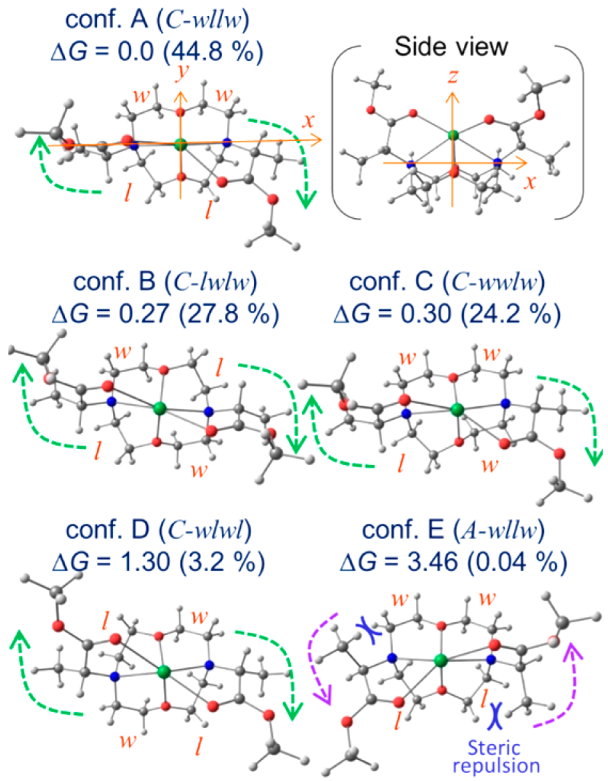

Figure 1. Structures of five lowest conformers of Eu^{3+}−DODP complex. Gibbs free energies (in kcal/mol) and existing probabilities (in %) are calculated at 245.15 K and 1 atom. Green and purple arrows indicate the direction of ester arms, clockwise (*C*) and anticlockwise (*A*), respectively. "*l*" (lengthwise) and "*w*" (widthwise) represent the directions of the C_2 units in the 12-membered ring.

DOI: 10.1021/acscatal.5b00438
ACS Catal. 2015, 5, 3731−3739

The differences among these conformers come from the direction of two esters and the structures of 12-membered ring. We analyze the differences among the lowest five conformers **A**−**E** in detail. The major difference between the conformers **A**−**D** and the conformer **E** is in the direction of two esters. As seen in Figure 1, in the conformers **A**−**D**, two esters (more specifically their NCC═O arms) are stretched clockwise (*C*, as shown in green arrows) above the 12-membered ring, and for the conformer **E**, they are anticlockwise (*A*, purple arrow). The difference among the conformers **A**−**D** is in the structures of 12-membered rings. The structure of the 12-membered ring can be categorized by the directions of four C_2 units, lengthwise (*l*) and widthwise (*w*), as seen in the structures in Figure 1. The conformation **A**, for instance, has a *wllw* combination for the 12-membered ring (starting from the upper right C_2 unit and moving clockwise) and has two esters stretched clockwise (*C*), and thus can be identified having *C-wllw* conformation. **B** has *C-lwlw*, **C** *C-wwlw*, and **D** *C-wlwl*. Conformation **E** has *A-wllw*. All the possible combinations of *A*/*C* and *w*/*l* are listed as conformers **A**−**T** in Table S1 and Figure S2.

The energy differences among the 20 conformers can be understood by two factors. First is the direction of the ester arms. The conformer **A**, with the two ester arms stretched clockwise is lower in energy than **E** with anticlockwise arms by 3.5 kcal/mol. The relative instability of **E** is due to the steric repulsion between a methylene group in 12-membered ring and the methyl group on the chiral carbons. As shown in Figure 1, in **E** there are two pairs of methylene-methyl close contact that makes this conformation less stable. This trend can be seen in other conformers and the anticlockwise group on the average is less stable than clockwise group by 1.9 kcal/mol. Second is the structural distortion of the 12-membered ring. As discussed in detail in the SI and shown in eqs S1 and S2, the relative electronic energies of clockwise conformers and anticlockwise conformers were found to be approximately represented by the summation of the energies of two C_2 units, such as *lw*, *wl*, *ww*, and *ll*, defined in Figure S3. Roughly speaking, for clockwise conformers the electronic energies of the *wl*, *ww*, and *ll* units are 0.8, 2.2, and 3.5 kcal/mol higher than the *lw* unit, respectively. For anticlockwise conformers, those of the *lw*, *ww*, and *ll* are 0.3, 1.9, and 3.6 kcal/mol higher than the *wl*, respectively. The reason for less stability of the *ww* and *ll* units can be explained by the geometrical distortion of the 12-membered ring. For instance, the C−O−C angles in conformers B(*C-lwlw*), D(*C-wlwl*), K(*C-wwww*), O(*C-llll*) are 114−115°, 114−115°, 111−112°, 119°, respectively. These angles are distorted most in the *llll* structure, followed by the *wwww* structure, compared with the *lwlw* and *wlwl* structures. The energy difference between the *lw* and *wl* units is caused by the steric repulsion between 12-membered ring and the ester arms. As shown in Figure S4, the distances between H atoms are shorter in *lw* for clockwise and *wl* for anticlockwise structure. Therefore, the *lw* and *wl* units have higher electronic energies in clockwise and anticlockwise structures, respectively. Note that the analyses above are based on the electronic energies. The Gibbs free energies (shown in Figure 1) are determined by electronic energies and a few kcal/mol of relative entropic effects that relate to the flexibility of the structures (Table S1).

The energy differences among the conformers **A**, **B**, and **C** are less than 0.3 kcal/mol, and their Boltzmann distributions at 248.15K condition are comparable (i.e., 45%, 28%, and 24%); the Boltzmann distributions of other conformers are a total of 3%. Therefore, we can say that the three conformers **A**, **B**, and **C** coexist under the experimental condition. This is a quite rare situation that more than two conformers of chiral catalysts coexist and still achieve high stereoselectivity. In the following sections, we will consider all the three conformers **A**, **B**, and **C**. Note that the barriers for the conformational change from **A** to **C** and from **C** to **B** are 6.4 and 5.1 kcal/mol, respectively (Figure S5). This means that the existing probabilities of the conformers **A**, **B**, and **C** should be determined thermodynamically because of the low conformational barriers.

Coordination of Aldehyde and Water to Eu^{3+}−DODP Catalyst. According to the luminescence decay measurement,[22−24] on the prereaction complex, Eu^{3+} is coordinated by one benzaldehyde and two water molecules. Starting from the stable conformations of Eu^{3+}−DODP, **A**, **B**, and **C**, we optimized the structures of Eu^{3+}−DODP complexes coordinated with one benzaldehyde and two water molecules. Figure 2 shows the most stable coordination structure **IntB1**, obtained from the conformer **B**. In **IntB1**, two water molecules coordinate to Eu^{3+} from +*z* and +*y* directions, and one

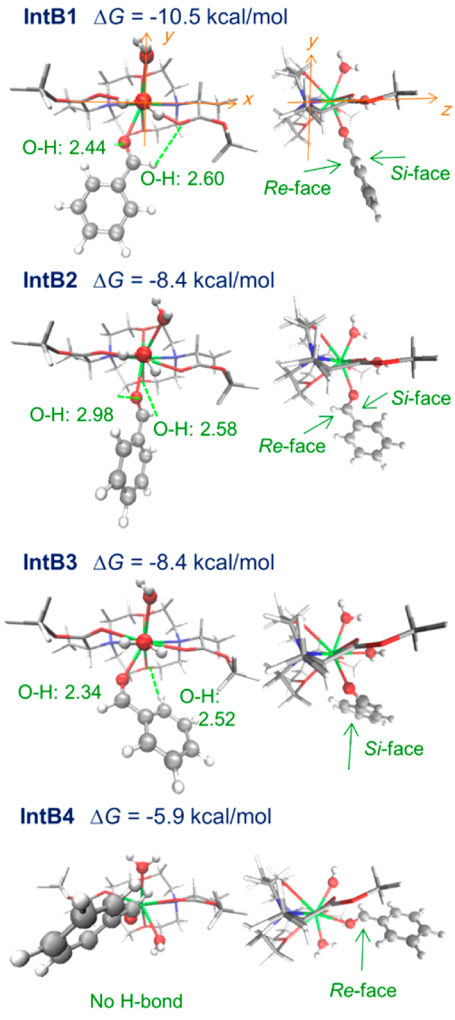

Figure 2. Stable coordination structures (top and side views) of the reactant complex between benzaldehyde and two water molecules with the catalyst conformer **B**. The Gibbs free energies (in kcal/mol, relative to **A** plus isolated benzaldehyde and two water molecules) are calculated at 245.15 K and 1 atom condition. The bond distances are in Å. Labels "*Re-face*" and "*Si-face*" indicate that these faces of coordinated benzaldehyde is open for further attack.

DOI: 10.1021/acscatal.5b00438
ACS Catal. 2015, 5, 3731−3739

aldehyde coordinates from $-y$ direction. The benzaldehyde is positioned not only by Eu^{3+} but also by the ligand through two hydrogen bonds, as shown in Figure 2. In this structure, both *Re*-face and *Si*-face attacks of silyl enol ether seem to be possible. Thus, the enantioselectivity cannot be determined by the structure of the most stable prereaction complex. The structures and energies of the TSs for the stereodetermining step must be studied to discuss the stereoselectivity.

In other coordination structures, **IntB2** and **IntB3**, the free energies are 2.1 kcal/mol less stable than **IntB1**, although the coordination pattern is similar to **IntB1**. The reason for lower stability of **IntB2**−**B3** can be understood by their structures and the energy decomposition analyses (EDA)[46,47] shown in Table S2. Although benzaldehyde is on $-y$ direction in all **IntB1**−**B3**, the hydrogen bond networks between aldehyde and the ligand are different. In **IntB1**, two hydrogen bonds are formed between benzaldehyde and the ligand. **IntB2** has only one hydrogen bond, which causes the weaker electrostatic interaction. **IntB3** has a lower electronic energy than **IntB1** because of the stronger hydrogen bonds. However, the free energy of **IntB3** is less stable than **IntB1** because of the entropic effect from tighter binding of benzaldehyde. These hydrogen bond networks can be reorganized very easily. For instance, the barrier from **IntB1** to **IntB3** is only 3.4 kcal/mol (Figure S7). In another coordination structure, **IntB4**, benzaldehyde coordinates from $+z$ direction and two water molecules coordinate from $+y$ and $-y$ directions. In this structure, no hydrogen bond can be formed, which causes weaker electrostatic interaction.

Similar coordination structures to the conformers **A** and **C** were also obtained. (**IntA1**−**A4**, **IntC1**−**C4** in Figure S6.) The most stable coordination structures obtained from **A** and **C** (**IntA1** and **IntC1**) are only 0.3 and 0.4 kcal/mol less stable than **IntB1**, respectively. Other coordination structures **IntA2**−**A4** and **IntC2**−**C4** are less stable, and the reason for lower stability can be explained in a similar fashion to those of **IntB2**−**B4**, considering the EDA and the entropic effect, as shown in Table S2. The barrier for the conformational change of the ligand part is affected little by the coordination of benzaldehyde and water molecules. The barriers among **IntA1**, **IntB1**, and **IntC1** are similar to those among **A**, **B**, and **C** as shown in Figure S7.

Transition States of the C−C Bond Formation Step. As mentioned in the previous section, we cannot predict the major stereoisomer from the structure of the most stable prereaction complex, because there is enough space for both *Re*- and *Si*-face attacks of silyl enol ether. Thus, in this section, we focus on the C−C bond formation step between benzaldehyde and silyl enol ether in the present Ln complex. The Aldol product has four stereoisomers, (*R*,*R*), (*S*,*S*), (*R*,*S*), and (*S*,*R*), which are determined by the approach direction and the molecular plane of the silyl enol ether, as shown in Figure 3. To find all the possible TSs for the C−C bond formation, the TSs were searched exhaustively by using the MC-AFIR method starting from *initial* structures in which the approach direction and orientation between the lower prereaction complexes, **IntA1**−**A3**, **B1**−**B3**, and **C1**−**C3**, and the silyl enol ether are sampled randomly, as described in the Computational Detail section. Here (and later) we use "the approach direction" to mean from which direction the silyl enol ether substrate approaches a fixed catalyst prereaction complex, which is equivalent to the direction of the vector connecting the two reacting carbon atoms. With "the orientation", we mean the orientation of the

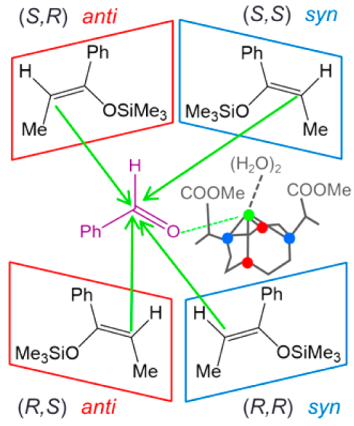

Figure 3. Schematic procedure of the MC-AFIR calculation. The artificial force was added between two reacting carbon atoms (shown with green arrows), with different silyl enol ether approaches for the four stereoisomers, (*R*,*R*), (*R*,*S*), (*S*,*S*), (*S*,*R*), respectively, and the random initial structures were sampled for different approach directions and substrate orientations.

substrate molecule relative to the fixed prereaction complex. As a result of exhaustive search, 19 (*R*,*R*), 14 (*S*,*S*), 13 (*R*,*S*), and 18 (*S*,*R*) unique TSs leading to different product enantiomers were obtained. The AFIR search successfully sampled (without expensive molecular dynamics simulation) TSs not only for the conformations of the forming C−C bond but also for the relative orientations among the Eu^{3+}−DODP catalyst, benzaldehyde, and silyl enol ether. Figure 4a shows the distribution of relative free energy as functions of the C−C−C−O dihedral angle ϕ defined in Figure 4b of the obtained TSs. Detailed structural parameters are shown in Table S4. The lowest TS, named (*R*,*R*)-**TSB1**, gives the (*R*,*R*) product and has the activation energy of 9.44 kcal/mol from **IntB1** + silyl enol ether. This activation energy is higher than the barriers for the conformational changes among **A**, **B**, and **C** or among **IntA1**, **IntB1**, and **IntC1**. Thus, as described in the Curtin−Hammett principle,[48] the ratios of stereo products can be determined only by the free energy differences of the TSs of the C−C bond formation step. The C−C dihedral angle ϕ of all the TSs is localized around 60°, 180°, 300°, which means all the TSs have the staggered (*trans* and *gauche*) C−C conformations. The stereo ratios were calculated by considering the Boltzmann distributions of all the obtained TSs at 248.15 K and 1 atom. The existing probabilities of the TSs producing (*R*,*R*), (*S*,*S*), (*R*,*S*), and (*S*,*R*) are 94.7%, 3.7%, 0.4%, and 1.2%, respectively. The calculated diastereomeric ratio is *syn* [(*R*,*R*)+(*S*,*S*)] 98.4%/*anti* [(*R*,*S*)+(*S*,*R*)] 1.6% and the enantiomeric excess, [(*R*,*R*)-(*S*,*S*)]/[(*R*,*R*)+(*S*,*S*)], is 92.5% *ee* (*syn*), and both agree very well with the experimental values,[22,23] 97%: 3% and 93% *ee* (*syn*).

Among the obtained TSs, only one TS, (*R*,*R*)-**TSB1**, has a notably low free energy, and the others have energies more than 1.4 kcal/mol higher, as shown in Figure 4a. This feature is quite different from that in our previous study[38,39] on the same reaction catalyzed by $Eu^{3+}(H_2O)_8$. In the case of the $Eu^{3+}(H_2O)_8$-catalyzed reaction, there existed many TSs whose energies were comparable because of the fluctuation of coordination water molecules around Eu^{3+}as well as the torsion around the forming C−C bond; this geometrical fluctuation around Eu^{3+} was one of the reasons of the low stereoselectivity. In the present case the of Eu^{3+}−DODP-catalyzed reaction, the

DOI: 10.1021/acscatal.5b00438
ACS Catal. 2015, 5, 3731−3739

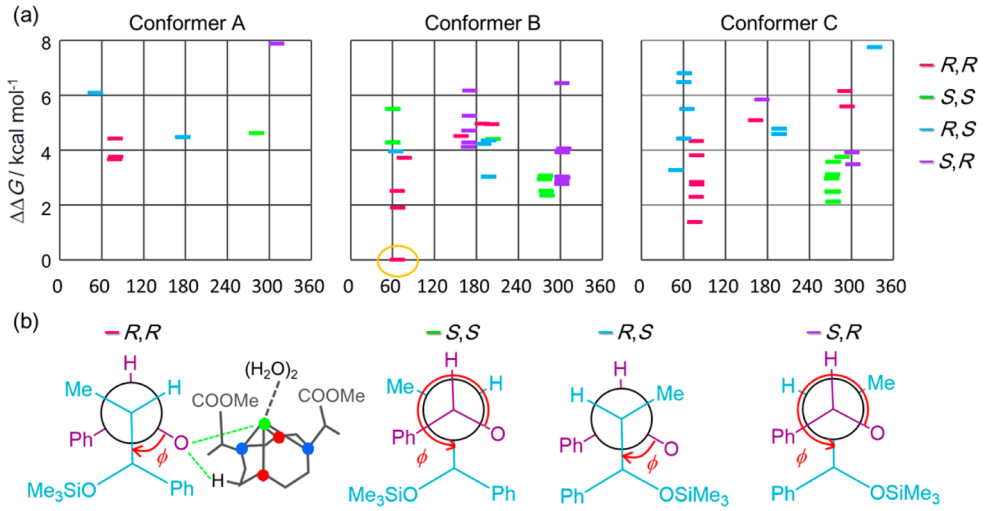

Figure 4. (a) Distribution of the TSs for the C−C bond formation step involving conformers **A**, **B**, and **C**. Pink, green, blue, and purple lines represent (*R*,*R*), (*S*,*S*), (*R*,*S*), and (*S*,*R*) TSs, respectively. The vertical axis is the Gibbs free energy difference (in kcal/mol) from the most stable TS (shown in the orange circle) with the activation energy of 9.44 kcal/mol. The horizontal axis is the dihedral angle around the forming carbons (<C−C−C−O) defined in (b).

geometrical fluctuation around Eu^{3+} is reduced by the ligand, especially by the H-bond network between the substrates and the ligand, which is one of the factors for the high stereoselectivity.

Now, we focus on the geometry of the TSs producing the major (*R*,*R*) product. As shown in Figure 5a, (*R*,*R*)-**TSB1** has

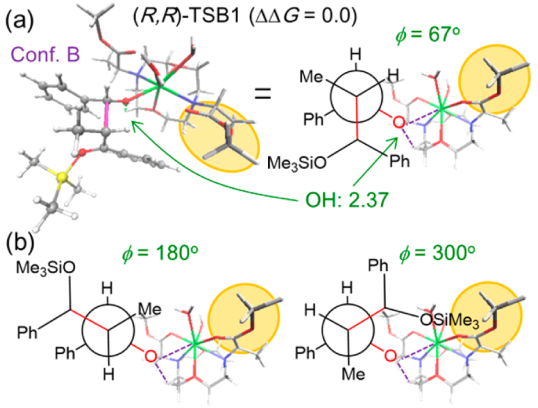

Figure 5. (a) The structure and Newman projection of the lowest (*R*,*R*)-**TSB1** obtained for the conformer **B**. Bond distance is in Å. The reactive C−C bond and the steric part in the ligand are represented as a pink line and an orange circle, respectively. The activation energy is 9.44 kcal/mol from **IntB1** + silyl enol ether. (b) Newman projections of different orientations.

an ideal structure in which all the bulky groups, such as phenyl and TMS groups in the substrates and ester parts in the catalyst, avoid each other to reduce the steric repulsion. (Other side views are in Figure S8.) This TS is obtained from the lowest complex **IntB1** in Figure 2; the Eu^{3+} catalyst retained the conformation **B** at this TS. The hydrogen bond between the oxygen in benzaldehyde and the hydrogen in the 12-membered ring (2.44 Å in **IntB1**) is kept in this TS (2.37 Å). However, the weaker hydrogen bond between α-H in benzaldehyde and the oxygen in the ester arm (2.60 Å in **IntB1**) is broken, and benzaldehyde rotates about 90° to accommodate the *Re*-face attack of the silyl enol ether. In (*R*,*R*)-**TSB1**, the C−C dihedral angle ϕ is 67°. (*R*,*R*)-TSs with $\phi \approx 60$ ° are more stable than those with $\phi \approx 180$° and 300°. For instance, as shown in Figure 4, (*R*,*R*)-TSs with $\phi \approx 180$° are 4−5 kcal/mol higher than those with $\phi \approx 60$ °. Those TSs with $\phi \approx 300$ ° are even higher in energy. The reason for the favorable orientation in (*R*,*R*)-**TSB1** between two substrates can be understood by the Newman projection shown in Figure 5b. (*R*,*R*)-**TSB1** has the dihedral angle ϕ = 67° in which the small hydrogen in the silyl enol ether faces to the bulky part in the ligand (shown in the orange circle in Figure 5). In other orientations ϕ = 180 ° and 300°, the bulky part is near the methyl and TMS groups, respectively. Therefore, those are less stable due to the steric repulsion between the ligand and the silyl enol ether.

The most stable (*R*,*R*) TSs with the conformers **A** and **C** also have similar orientations ($\phi \approx 60$°). For instance, the second lowest (*R*,*R*) TS, (*R*,*R*)-**TSC1**, is obtained from the conformer **C**. However, their energies are more than 1.4 kcal/mol higher than the lowest (*R*,*R*) TS with the conformer **B**. As shown in Table S3, the (*R*,*R*)-**TSC1** is higher than (*R*,*R*)-**TSB1** in Gibbs free energy but lower in electronic energy; the instability of (*R*,*R*)-**TSC1** (as well as **TSA1**) comes from the entropic destabilization. The reason for the entropic destabilization can be understood by the smaller space available for the reactants. In (*R*,*R*)-**TSC1** structure, as shown in Figure S9, the ester arm (in an orange circle) is leaned more than that of (*R*,*R*)-**TSB1**. Thus, to avoid the steric repulsion between the ester arm and the phenyl group in the silyl enol ether, the dihedral angle around the reactive C−C bond (ϕ) becomes 77 ° which is 10° larger than (*R*,*R*)-**TSB1**. Therefore, we can say that the space for substrates for (*R*,*R*)-**TSC1** is smaller than that for (*R*,*R*)-**TSB1**, which results in less flexibility of the structure, in other words, larger entropic destabilization. The (*R*,*R*) TSs obtained from the conformer **A** has also smaller space than (*R*,*R*)-**TSB1** (and **TSC1**), which results in lower stability.

Here, the reasons for the two experimental facts[22,23] mentioned in the Introduction can be understood from the structure of (*R*,*R*)-**TSB1**. First, the product yield depends on the substituents on two ester arms in the ligand ("R" in Scheme 1). Too bulky substituents (R) should cause too small space for substrates, which results in low reactivity and selectivity.

DOI: 10.1021/acscatal.5b00438
ACS Catal. 2015, 5, 3731−3739

Second, highly stereoselectivity was achieved both for aromatic and aliphatic aldehydes. The phenyl group of the benzaldehyde is located far enough from the ligand. Thus, the substituent of the aldehyde should not affect the structure of the lowest (*R*,*R*) TS. The third point, the lanthanide dependency, is discussed in the following section.

The most important role of the chiral catalyst is controlling enantioselectivity that means the approach direction of the silyl enol ether. Therefore, we now focus on the (*S*,*S*) TSs that produce the enantiomer of the major product (*R*,*R*). The lowest (*S*,*S*) TS, (*S*,*S*)-**TSC3**, is derived from **IntC3** (shown in Figure S6. The position of benzaldehyde in **IntC3** is similar to **IntB3** in Figure 2.). In **IntC3** (as well as **IntB3**), *Re*-face attack is blocked by the ligand, and only *Si*-face attack is possible. The smaller stability of (*S*,*S*) TSs compared to (*R*,*R*)-**TSB1** comes from the smaller stability of **IntC3** vs **IntB1**. The reason for smaller stability of **IntC3** vs **IntB1** is the same as that of **IntB3** vs **IntB1**, which, as discussed before, is the entropic destabilization of the former due to the tighter bonding of benzaldehyde with the ligand. (See Tables S1 and S2.) The orientation between benzaldehyde and silyl enol ether in the (*S*,*S*)-**TSC3** is similar to that of (*R*,*R*)-**TSB1**, and only the approach direction of silyl enol ether is opposite as shown in Figure 6a. In this orientation (ϕ = 274°), the hydrogen in the silyl enol ether faces to the bulky part of the ligand. Therefore, other orientations, such as $\phi \approx 60°$ and 180°, are less stable due to the steric repulsion between the bulky part of the ligand and methyl and TMS groups, respectively. Note that the bulky part of the ligand for (*S*,*S*)-**TSC3** is the ester arm on the left side, whereas that for (*R*,*R*)-**TSB1** is the ester arm on the right side as shown in Figure 5a and 6a.

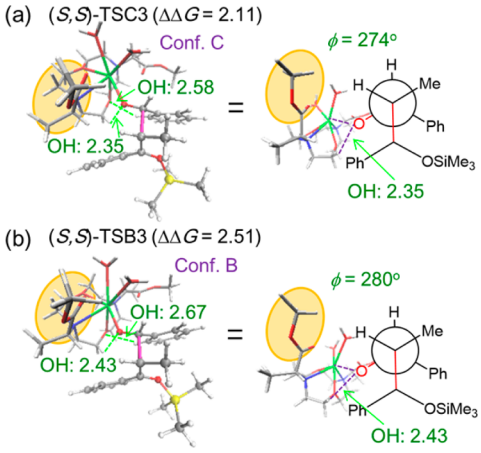

Figure 6. Structures and Newman projections of (a) the lowest (*S*,*S*) TS, (*S*,*S*)-**TSC3**, and (b) (*S*,*S*)-**TSB3**. The Gibbs free energies are in kcal/mol. Bond distances are in Å. The reactive C−C bond and the steric part in the ligand are represented as a pink line and an orange circle, respectively.

To clarify the influence of the conformation of the catalyst on the stability of (*S*,*S*) TSs, we compare the structures of (*S*,*S*) TSs obtained by the conformers **C** and **B**. As shown in Figure 6b, (*S*,*S*)-**TSB3**, the lowest (*S*,*S*) TS with **B** conformation, is obtained from the conformer **B** (**IntB3**, which is 0.78 kcal/mol less stable than **IntC3**). The energy difference between (*S*,*S*)-**TSC3** and (*S*,*S*)-**TSB3** is only 0.40 kcal/mol. Their structures and orientations are similar, and the dihedral angles for (*S*,*S*)-**TSC3** and (*S*,*S*)-**TSB3** are ϕ = 274° and 280°, respectively. The energy difference comes from different hydrogen bond distances, which is slightly shorter in (*S*,*S*)-**TSC3**, as shown in Figure 6.

Next, the diastereomers of (*R*,*R*) and (*S*,*S*) structures are discussed. In (*R*,*S*) TS structures, which are the diastereomer of (*R*,*R*), the silyl enol ether approaches the benzaldehyde from the same direction with the opposite molecular plane. The most stable (*R*,*S*) TS, (*R*,*S*)-**TSB1** is obtained from the conformer **B** (**IntB1**), and its orientation is ϕ = 198°. The favorable orientation can be understood in a similar fashion. As shown in Figure S10, the hydrogen in the silyl enol ether faces to the bulky part of the ligand for $\phi \approx 180°$, while methyl and phenyl groups face to the bulky part for $\phi \approx 60°$ and 300°, respectively. Thus, the steric repulsion causes less stability for $\phi \approx 60°$ and 300°. The lowest (*R*,*S*) TS is 3.03 kcal/mol less stable than (*R*,*R*)-**TSB1**. The major reason is the steric repulsion between the phenyl group in the silyl enol ether and the ester arm of the ligand. (See the EDA in Table S3.) The diastereomer of (*S*,*S*), (*S*,*R*) TS, is also less stable than (*R*,*R*)-**TSB1**. Figure S11 shows the lowest (*S*,*R*) TS whose Gibbs free energy is 2.76 kcal/mol higher than (*R*,*R*)-**TSB1**. The coordination structure of the benzaldehyde is the same as **IntB3**. Thus, the reason for the lower stability is the same as (*S*,*S*)-**TSC3** and (*S*,*S*)-**TSB3**—the entropic destabilization due to the tighter bonding of benzaldehyde with the ligand.

As shown above, the reason for the largest stability of (*R*,*R*)-**TSB1** (or lower stability of other TSs) can be understood as follows. The lower stability of the (*S*,*S*) and (*S*,*R*) TSs is caused by the entropic destabilization due to too tight hydrogen bonds between benzaldehyde and the ligand. This destabilization also causes the lower stability of their prereaction complexes **IntC3** or **IntB3** compared with **IntB1**. The lower stability of the (*R*,*S*) TSs comes from the steric repulsion between the ligand and the silyl enol ether. In summary, the chiral ligand has two roles. One is the fixing of the position of benzaldehyde by the hydrogen bonds. Although excessively tight hydrogen bonds sometimes cause the lower stability, for instance, in (*S*,*S*) and (*S*,*R*) TSs, appropriate hydrogen bonds stabilize the TSs as well as prereaction complexes, and they keep the oxygen in the benzaldehyde near the hydrogen atom in the 12-membered ring. As a result, benzaldehyde is kept in the space surrounded by two ester arms, which blocks the approach of bulky parts of the silyl enol ether.

How To Improve the Enantioselectivity. The most important role of the computational chemistry is gaining new insights for improving the reaction, such as achieving higher yield and stereoselectivity, or performing under milder condition. Here, we discuss a strategy to improve the enantioselectivity. As shown in the previous section, the lowest TS which produces the major (*R*,*R*) structure is obtained from the conformer **B**, while the lowest (*S*,*S*) TS, enantiomer of (*R*,*R*), is obtained from the conformer **C**. There are (*S*,*S*) TSs obtained from the conformer **B**, but the Gibbs free energy is 0.4 kcal/mol higher than the lowest (*S*,*S*) TS. Therefore, we can say that the enantioselectivity should be higher if the conformer **C** does not exist in the reaction system. In other words, a strategy to improve the enantioselectivity is reducing the probability of conformer **C** as well as increasing that of **B**. To change the existing probability of conformers, we changed Eu^{3+} to another Ln^{3+}. The difference among Ln^{3+} (Ln = La − Ln) is the number of in-core 4f electrons. As mentioned in the Introduction, the 4f electrons do not form a covalent bond with the ligands because they are shielded by the closed-shell 5s and

DOI: 10.1021/acscatal.5b00438
ACS Catal. 2015, 5, 3731−3739

5p electrons from outside. Thus, the bonding character is quite similar among different Ln complexes, and only the ionic radii of Ln^{3+} are different; the radius decreases nearly linearly from 1.03 Å in La^{3+} to 0.86 Å in Lu^{3+}.[49]

Figure 7 shows the existing probabilities of the conformers **A**–**D** with Ln^{3+} (Ln = La – Lu), calculated from the free

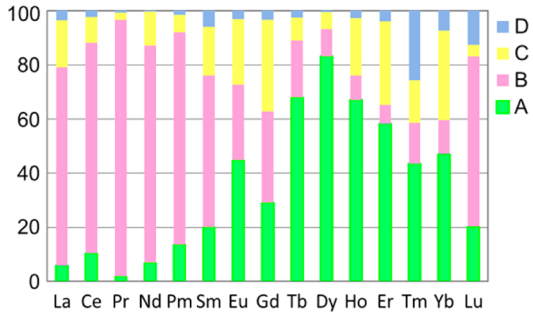

Figure 7. Existing probabilities (in %) of the conforms **A**–**D** with different Ln^{3+} (Ln = La – Lu).

energies at the present level of theory. The existing probability of the conformer **B** increases and that of **C** decreases, as the atomic number of Ln^{3+} decreases. For Ln = Pr, the conformers **B** and **C** have the largest and smallest existing probabilities, respectively. This is consistent with the experimental fact[23] that the enantioselectivity is the highest for Ln = Nd, which is the next to Pr. The difference of ionic radii between Pr^{3+} and Nd^{3+} is only 0.01 Å.[49] Therefore, we can say that one way to improve the enantioselectivity is reducing the probability of the conformers that form stable TSs producing minor stereo isomers.

The reason for the Ln dependency is discussed in the SI (see Figures S12–S15). First, the reason for the decrease of the conformer **B** and increase of **A** from early to middle Ln can be explained by the deformation of the ligand part, especially the distortion of the angles around the O atoms in the 12-membered ring. The distortion of some of angles in **A** become smaller as the atonic number of Ln^{3+} increases, while the distortion of all the angles in **B** become larger. Thus, the conformer **B** becomes less stable than **A** as the atomic number of Ln^{3+} increases. Second, the decrease of the conformer **A** in late Ln comes from the entropic destabilization effect of **A**, which is the smallest for Ln = Dy. Third, the reason for the largest existing probability of the conformer **B** for Ln = Pr can be explained by the smallest distortion of the angles around O atoms in the 12-membered ring as well as the smallest entropic destabilization. Though it is difficult to explain the reason for the smallest entropic destabilization, these analyses imply that Eu^{3+} should be too small to hold the ligand, and Pr^{3+} fits the best among the Ln^{3+}. We notice in Figure 7 that Lu appears to not follow the trends of the other lanthanides. Although it is difficult to show the evidence, we can guess a reason for this deviation, as discussed on p S16 in the SI.

CONCLUSIONS

In this study, we focused on the stereoselective aqueous Mukaiyama-Aldol reaction catalyzed by the chiral Eu^{3+}–DODP complex and clarified the origin of the stereoselectivity by using the Global Reaction Root Mapping (GRRM) strategy. At first we showed that, although typical chiral catalysts had only one rigid conformer, the Eu^{3+}–DODP catalyst had three conformers **A**, **B**, and **C**, all with large existing probabilities. These three conformers had similar structures, and only the conformations of the 12-membered rings are different. Next, we examined the prereaction complexes where one benzaldehyde and two water molecules are coordinated to the conformers **A**–**C**, using the coordination number from the previous luminescence measurements.[22−24] The most stable prereaction complex **IntB1** was obtained from the conformer **B**, where the oxygen atom of benzaldehyde was positioned between Eu^{3+} and a hydrogen atom of the 12-membered ring. Other prereaction complexes are less stable because of the weaker electrostatic interaction or entropic destabilization. The most stable prereaction complex **IntB1** has space both for *Re*- and *Si*-face attacks. The position of benzaldehyde in the stable prereaction complexes from the conformers **A** and **C** are similar to those from **B**.

In order to discuss the enantioselectivity, the transition states (TSs) of the stereodetermining C–C bond formation were explored exhaustively by using the artificial force induced reaction (AFIR) method based on the obtained prereaction complexes. The enantio excess and diastereomeric ratio were evaluated using the 64 optimized TSs and the results reproduced the experimental ratios quantitatively. The 12-membered ring and bulky ester arms in the ligand play an essential role in controlling the stereoselectivity. The 12-membered ring keeps the position of the benzaldehyde by the hydrogen bond network. The bulky ester arms restrict the relative orientation of the ligand, benzaldehyde, and silyl enol ether by blocking the approach of the bulky parts in the silyl enol ether.

The obtained TS structures explain three experimental facts about the dependency on the ligand substituents and on lanthanides, as well as the independency on the aldehyde substituent. First, the substituents on the ligand determine the size of the space for two substrates. Thus, too large substituents should cause the difficulty in coordinating the benzaldehyde and in approach of the silyl enol ether. Second, the substituents on aldehydes are far enough from the catalyst, so they should not affect the structure of the TSs for the C–C bond formation step.

Third, the lanthanide controls the existing probability of each conformer. By using Ln^{3+} having larger ionic radius, such as Pr^{3+}, the conformation around Ln^{3+} becomes less flexible and only one of the conformers, **B**, has a large existing probability. To improve the enantioselectivity, the conformer **C** has to be reduced because it forms the lowest (*S*,*S*) TS which is the enantiomer of the major stereo isomer (*R*,*R*). The enantioselectivity can be improved by replacing Eu^{3+} by larger Ln^{3+}, which is consistent with the experimental fact that Nd^{3+} catalyst achieved the highest enantioselectivity.[23] This strategy is totally different from the conventional one for rigid chiral catalysts. For conventional rigid chiral catalysts, there are two ways to improve stereoselectivity. One is using bulkier substituents to block the approach of substrates. Another is making stronger $\pi-\pi$ or hydrogen bond interaction between ligand and substrates to keep the position and orientation of substrates. However, the way to improve stereoselectivity for *flexible chiral* catalysts, such as Ln^{3+}–DODP, would be reducing the existing probabilities of conformers that result in the formation of minor stereo isomers We believe that this is the first study which elucidates the origin of stereoselectivity and strategy to improve it for flexible chiral catalyst. This information should be useful in developing chiral ligands used in aqueous media.

DOI: 10.1021/acscatal.5b00438
ACS Catal. 2015, 5, 3731–3739

COMPUTATIONAL DETAILS

First, we explored the local minimums (LMs) of the catalyst without water and substrate by using the ADDF method[41−43] at PM6 level of theory[50] At this moment, Eu^{3+} was replaced by Lu^{3+} because its PM6 parameters were not available in Gaussian 09,[51] and the ionic radius of Lu^{3+} (0.97 Å) is similar to that of Eu^{3+}(1.07 Å).[49] Then, the large-ADDF (*l*-ADDF) search was performed for six largest ADD directions starting from a LM, conformer **D** in Figure 1, and continued until no new LM was found whose energy was lower than those of 20 lowest LMs already found. As a result, 24 LMs of the Lu^{3+}−DODP complex were found. Because *l*-ADDF finds all the LMs of a given system connected by low isomerization barriers, it is unlikely that any structure that would have significant Boltzmann population has been missed in the preset search.

Second, starting from all the 24 LMs of Lu^{3+}−DODP complex found by ADDF with PM6 above, standard optimization of Eu^{3+}−DODP was performed at the dispersion-corrected B3LYP-D3 level,[52−54] including the solvation effect by the polarized continuum (PCM) model[55,56] with a dielectric constant of 78.3553 (water). Eu^{3+} was described by using the Stuttgart-Dresden large-core relativistic effective core potential (RECP)[57,58] throughout, where the 5s, 5p, 5d, 6s electrons were considered explicitly and six 4f electrons were included in the RECP. The basis sets for the geometry optimizations were (7s6p5d)/[5s4p3d] RECP basis set for Eu^{3+}, 6-31+G* for O and N, and 6-31G* for C and H (BS1). The single-point calculations were performed at the B3LYP-D3 theory with (8s7p6d3f2g)/[6s5p5d3f2g] RECP basis set[59] for Eu^{3+} and cc-pVTZ for others (BS2). The geometries were optimized for the electronic energy. The Gibbs free energies were evaluated using the Gibbs free energy correction terms. Among the obtained structures, only three lower LMs, **A**, **B**, and **C** in Figure 1, have Boltzmann distributions at 248.15 K and 1 atom larger than 5% and were considered for the following stages. Note that although the structure of each conformer with Lu^{3+} is similar to that of Eu^{3+}, the relative energies among the conformers depend on size of Ln^{3+} as mentioned above.

Next, the water and benzaldehyde coordinated structures were considered. According to the luminescence decay measurement, two water molecules and one benzaldehyde coordinate to Eu^{3+} catalyst.[22−24] Thus, the coordinated structures were examined by the AFIR method with adding artificial force between Eu^{3+} and oxygen atoms of two water molecules and one benzaldehyde. To reduce computational cost, the AFIR search was performed at the B3LYP-D3 level with small basis sets, (7s6p5d)/[2s1p1d] for Eu^{3+} and 6-31G for others (BS3). The obtained approximate LMs were fully reoptimized without artificial force at B3LYP-D3 with BS1 basis set and single-point calculations are performed with the BS2 basis set.

Finally, the origin of the stereoselectivity was examined. We have already studied the whole mechanism of aqueous Mukaiyama-Aldol reaction catalyzed by $Eu^{3+}(H_2O)_8$ in ref 39 and clarified that the reaction starts from C−C bond formation, which was the stereodetermining step, followed by proton transfer and TMS dissociation. Although the ligand and substituents in the silyl enol ether are different from the systems in the present work, most parts are quite similar, such as the coordination number around $Eu^{3+}$and aldehyde that coordinates to Eu^{3+} directly, and the present reaction should proceed in the same pathway as in the previous work. Therefore, to discuss the stereoselectivity of the current reaction, we focus only on the C−C bond formation step. The TSs for this step were at first exhaustively explored by the multicomponent (MC) AFIR method with addition of an artificial force between the two reacting carbon atoms, as shown in Figure 3. As mentioned below, **IntA1−3**, **B1−3**, and **C1−3** shown in Figures 2 and S6 were used as initial structures, and 250 starting structures were prepared and the coordination of TMS enol ether in each initial structure was determined randomly, as described in ref 44. For the MC-AFIR search of approximate TSs with artificial force, B3LYP-D3 with small basis set BS3 was used, and the true TSs were reoptimized at the same level of theory without artificial force starting from the approximate TSs. Among these TSs, only 64 TSs whose Gibbs free energy differences from the lowest TS are less than 5.0 kcal/mol were kept and reoptimized at the B3LYP-D3 with BS1 basis set. Then the single-point calculations were performed at the B3LYP-D3 with BS2 basis set. All these ADDF, AFIR, and reoptimization calculations were performed by the GRRM program[60] using energies and energy derivatives computed by the Gaussian09 program.[51]

ASSOCIATED CONTENT

Supporting Information

The Supporting Information is available free of charge on the ACS Publications website at DOI: 10.1021/acscatal.5b00438.

General information about Ln^{3+}−DOTA, conformations of the (*R*,*R*)-Eu^{3+}−DODP catalyst, conformational change among the conformers **A**−**C**, other prereaction complexes from the conformers **A** and **C**, energy decomposition analyses (EDA), structural parameters of the TSs of the C−C bond formation, comparison of (*R*,*R*) TSs with the conformers **A**−**C**, the structures of (*R*,*S*) and (*S*,*R*) TSs, detailed analyses for the Ln dependency, and Cartesian coordinates and absolute energies (PDF)

AUTHOR INFORMATION

Corresponding Authors

*E-mail: morokuma@fukui.kyoto-u.ac.jp.

*E-mail: hatanaka@chem.kindai.ac.jp.

Present Address

†Department of Chemistry, Faculty of Science and Engineering, Kinki University, Higashi-Osaka, Osaka 577-8502, Japan

Author Contributions

All authors have given approval to the final version of the manuscript.

Notes

The authors declare no competing financial interest.

ACKNOWLEDGMENTS

The authors are grateful to Prof. Satoshi Maeda of Hokkaido University for the GRRM code and discussions on the GRRM method. This work was partly supported by Grants-in-Aid from MEXT for Innovative Areas (Soft Molecular Systems, No. 26104519), for Young Scientist (B) (No. 26810005) to M.H., and for Scientific Research (No. 24245005, 26105733, and 15H02158) to K.M. at Kyoto University. M.H. acknowledges the Fukui Fellowship of Kyoto University and Collaborative Research Program for Young Scientists of ACCMS and IIMC,

DOI: 10.1021/acscatal.5b00438
ACS Catal. 2015, 5, 3731−3739

Kyoto University. The Computer resources at the Academic Center for Computing and Media Studies (ACCMS) at Kyoto University and Research Center of Computer Science (RCCS) at the Institute for Molecular Science are also acknowledged.

REFERENCES

(1) Li, C.-J. *Green Chem.* **2008**, *10*, 151−152.
(2) Pirrung, M. C. *Chem. - Eur. J.* **2006**, *12*, 1312−1317.
(3) Shaughnessy, K. H. *Chem. Rev.* **2009**, *109*, 643−710.
(4) Butler, R. N.; Coyne, A. G. *Chem. Rev.* **2010**, *110*, 6302−6337.
(5) Simon, M.-O.; Li, C.-J. *Chem. Soc. Rev.* **2012**, *41*, 1415−1427.
(6) *Aqueous-Phase Organometallic Catalysis*, 2nd ed.; Cornils, B., Herrmann, W. A., Eds.; Wiley-VCH: Weinheim, 2004.
(7) Kobayashi, S.; Manabe, K. *Acc. Chem. Res.* **2002**, *35*, 209−217.
(8) Kobayashi, S.; Nagayama, S.; Busujima, T. *J. Am. Chem. Soc.* **1998**, *120*, 8287−8288.
(9) Koito, Y.; Nakajima, K.; Kobayashi, H.; Hasegawa, R.; Kitano, M.; Hara, M. *Chem. - Eur. J.* **2014**, *20*, 8068−8075.
(10) Kobayashi, S. *Synlett* **1994**, *1994*, 689−701.
(11) Kobayashi, S.; Hachiya, I. *J. Org. Chem.* **1994**, *59*, 3590−3596.
(12) Kobayashi, S.; Sugiura, M.; Kitagawa, H.; Lam, W. W. L. *Chem. Rev.* **2002**, *102*, 2227−2302.
(13) Li, C.-J. *Chem. Rev.* **2005**, *105*, 3095−3165.
(14) Li, C.-J.; Chen, L. *Chem. Soc. Rev.* **2006**, *35*, 68−82.
(15) Lindström, U. M. *Chem. Rev.* **2002**, *102*, 2751−2722.
(16) Kobayashi, S. *Pure. Appl. Chem.* **2007**, *79*, 235−245.
(17) Kitanosono, T.; Kobayashi, S. *Adv. Synth. Catal.* **2013**, *355*, 3095−3118.
(18) Kitanosono, T.; Kobayashi, S. *Chem. Rec.* **2014**, *14*, 130−143.
(19) Mlynarski, J.; Baś, S. *Chem. Soc. Rev.* **2014**, *43*, 577−587.
(20) Nagayama, S.; Kobayashi, S. *J. Am. Chem. Soc.* **2000**, *122*, 11531−11532.
(21) Hamada, T.; Manabe, K.; Ishikawa, S.; Nagayama, S.; Shiro, M.; Kobayashi, S. *J. Am. Chem. Soc.* **2003**, *125*, 2989−2996.
(22) Mei, Y.; Dissanayake, P.; Allen, M. J. *J. Am. Chem. Soc.* **2010**, *132*, 12871−12873.
(23) Mei, Y.; Averill, D. J.; Allen, M. J. *J. Org. Chem.* **2012**, *77*, 5624−5632.
(24) Averill, D. J.; Allen, M. J. *Inorg. Chem.* **2014**, *53*, 6257−6263.
(25) Eliseeva, S. V.; Bünzli, J.-C. G. *Chem. Soc. Rev.* **2010**, *39*, 189−227.
(26) Bünzli, J.-C. G. *Chem. Rev.* **2010**, *110*, 2729−2755.
(27) Bünzli, J.-C. G.; Piguet, C. *Chem. Soc. Rev.* **2005**, *34*, 1048−1077.
(28) Aime, S.; Botta, M.; Ermondi, G. *Inorg. Chem.* **1992**, *31*, 4291−4299.
(29) Jacques, V.; Desreux, J. F. *Inorg. Chem.* **1994**, *33*, 4048−4053.
(30) Aime, S.; Botta, M.; Fasano, M.; Marques, M. P. M.; Geraldes, C. F. G. C.; Pubanz, D.; Merbach, A. E. *Inorg. Chem.* **1997**, *36*, 2059−2068.
(31) Caravan, P.; Ellison, J. J.; McMurry, T. J.; Lauffer, R. B. *Chem. Rev.* **1999**, *99*, 2293−2352.
(32) Dunand, F. A.; Aime, S.; Merbach, A. E. *J. Am. Chem. Soc.* **2000**, *122*, 1506−1512.
(33) Aspinall, H. C. *Chem. Rev.* **2002**, *102*, 1807−1850.
(34) Parker, D.; Dickins, R. S.; Puschmann, H.; Crossland, C.; Koward, J. A. K. *Chem. Rev.* **2002**, *102*, 1977−2010.
(35) Caravan, P.; Zhang, Z. *Eur. J. Inorg. Chem.* **2012**, *2012*, 1916−1923.
(36) Henriques, E. S.; Bastos, M.; Geraldes, C. F. G. C.; Ramos, M. J. *Int. J. Quantum Chem.* **1999**, *73*, 237−248.
(37) Cosentino, U.; Villa, A.; Pitea, D.; Moro, G.; Barone, V.; Maiocchi, A. *J. Am. Chem. Soc.* **2002**, *124*, 4901−4909.
(38) Hatanaka, M.; Maeda, S.; Morokuma, K. J. *J. Chem. Theory Comput.* **2013**, *9*, 2882−2886.
(39) Hatanaka, M.; Morokuma, K. *J. Am. Chem. Soc.* **2013**, *135*, 13972−13979.
(40) Maeda, S.; Ohno, K.; Morokuma, K. *Phys. Chem. Chem. Phys.* **2013**, *15*, 3683−3701.
(41) Ohno, K.; Maeda, S. *Chem. Phys. Lett.* **2004**, *384*, 277−282.
(42) Maeda, S.; Ohno, K. *J. Phys. Chem. A* **2005**, *109*, 5742−5753.
(43) Ohno, K.; Maeda, S. *J. Phys. Chem. A* **2006**, *110*, 8933−8941.
(44) Maeda, S.; Morokuma, K. *J. Chem. Phys.* **2010**, *132*, 241102−241106.
(45) Maeda, S.; Morokuma, K. *J. Chem. Theory Comput.* **2011**, *7*, 2335−2345.
(46) Morokuma, K. *J. Chem. Phys.* **1971**, *55*, 1236−1244.
(47) von Hopffgarten; Frenking, G. *WIREs Comput. Mol. Sci.* **2012**, *2*, 43−62.
(48) Seeman, J. I. *Chem. Rev.* **1983**, *83*, 83−134.
(49) Jia, Y. Q. *J. Solid State Chem.* **1991**, *95*, 184−187.
(50) Stewart, J. J. P. *J. Mol. Model.* **2007**, *13*, 1173−1213.
(51) Frisch, M. J.; Trucks, G. W.; Schlegel, H. B.; Scuseria, G. E.; Robb, M. A.; Cheeseman, J. R.; Montgomery, J. A.; Vreven, T.; Kudin, K. N.; Burant, J. C.; Millam, J. M.; Iyengar, S. S.; Tomasi, J.; Barone, V.; Mennucci, B.; Cossi, M.; Scalmani, G.; Rega, N.; Petersson, G. A.; Nakatsuji, H.; Hada, M.; Ehara, M.; Toyota, K.; Fukuda, R.; Hasegawa, J.; Ishida, M.; Nakajima, T.; Honda, Y.; Kitao, O.; Nakai, H.; Klene, M.; Li, X.; Knox, J. E.; Hratchian, H. P.; Cross, J. B.; Bakken, V.; Adamo, C.; Jaramillo, J.; Gomperts, R.; Stratmann, R. E.; Yazyev, O.; Austin, A. J.; Cammi, R.; Pomelli, C.; Ochterski, J. W.; Ayala, P. Y.; Morokuma, K.; Voth, G. A.; Salvador, P.; Dannenberg, J. J.; Zakrzewski, V. G.; Dapprich, S.; Daniels, A. D.; Strain, M. C.; Farkas, O.; Malick, D. K.; Rabuck, A. D.; Raghavachari, K.; Foresman, J. B.; Ortiz, J. V.; Cui, Q.; Baboul, A. G.; Clifford, S.; Cioslowski, J.; Stefanov, B. B.; Liu, G.; Liashenko, A.; Piskorz, P.; Komaromi, I.; Martin, R. L.; Fox, D. J.; Keith, T.; Laham, A.; Peng, C. Y.; Nanayakkara, A.; Challacombe, M.; Gill, P. M. W.; Johnson, B.; Chen, W.; Wong, M. W.; Gonzalez, C.; Pople, J. A. *Gaussian 09*, revision D.01; Gaussian, Inc.: Wallingford, CT, 2009.
(52) Lee, C. T.; Yang, W. T.; Parr, R. G. *Phys. Rev. B: Condens. Matter Mater. Phys.* **1988**, *37*, 785−789.
(53) Becke, A. D. *J. Chem. Phys.* **1993**, *98*, 5648−5652.
(54) Grimme, S.; Antony, J.; Ehrlich, S.; Krieg, H. *J. Chem. Phys.* **2010**, *132*, 154104−154119.
(55) Tomasi, J.; Mennucci, B.; Cammi, R. *Chem. Rev.* **2005**, *105*, 2999−3093.
(56) Scalmani, G.; Frisch, M. J. *J. Chem. Phys.* **2010**, *132*, 114110−114124.
(57) Dolg, M.; Stoll, H.; Savin, A.; Preuss, H. *Theor. Chim. Acta* **1989**, *75*, 173−194.
(58) Dolg, M.; Stoll, H.; Preuss, H. *Theor. Chim. Acta* **1993**, *85*, 441−450.
(59) Yang, J.; Dolg, M. *Theor. Chem. Acc.* **2005**, *113*, 212−224.
(60) *GRRM 14*: Maeda, S.; Harabuchi, Y.; Osada, Y.; Taketsugu, T.; Morokuma, K., Ohno, K.. http://grrm.chem.tohoku.ac.jp/GRRM/index_e.html.

DOI: 10.1021/acscatal.5b00438
ACS Catal. 2015, 5, 3731−3739